IEEE Access
Multidisciplinary | Rapid Review | Open Access Journal

Received August 23, 2020, accepted September 1, 2020, date of publication September 11, 2020,
date of current version September 23, 2020.

Digital Object Identifier 10.1109/ACCESS.2020.3023396

Synchronous Multi-Wavelength Ultra-Short-Pulse Laser With Arbitrary Wavelength Interval

RONGHUA LI[1], HUAI WEI[1], WEIXUAN QIN[1], ZEHANG MA[1], CHENGTIAN TANG[1], BIN LI[2], AND LI PEI[1]

[1]Key Laboratory of All Optical Network and Advanced Telecommunication Network, Ministry of Education, Institute of Lightwave Technology, Beijing Jiaotong University, Beijing 100044, China
[2]School of Information and Communication Engineering, Communication University of China, Beijing 100024, China

Corresponding author: Huai Wei (hwei@bjtu.edu.cn)

This work was supported by the National Key Research and Development Program of China under Grant 2018YFB1801003.

ABSTRACT Achieving multi-wavelength synchronous ultra-short pulses with arbitrary wavelength intervals is a difficult problem for fiber lasers. Herein, a laser based on multi-stage cascaded Mamyshev regenerators is proposed as a solution. The regenerators are cascaded to form a single laser cavity, each at a different position within the cavity and corresponding to a different output wavelength. A single pulse oscillating in the cavity has its wavelength sequentially switched by the regenerators. Synchronous multi-wavelength pulsed lasers with 5 nm and 0.01 nm output center-wavelength intervals are realized through numerical simulation; the output pulses have 10 nm spectral widths, peak powers of ∼0.7 kW, and durations of ∼0.4 ps. Design principles, system stability, and the effects of the filter bandwidth, length of single mode fiber and wavelength ordering in the cavity are discussed.

INDEX TERMS Fiber lasers, fiber nonlinear optics, laser mode locking, ultrafast optics.

I. INTRODUCTION

Thanks to short pulse durations and high intensities, ultra-short-pulse fiber lasers have become outstandingly important tools for various interdisciplinary applications [1]–[3]. Furthermore, as the field of application of these pulses has expanded, requirements for the properties of ultra-short-pulse lasers have become more stringent. In many applications, such as pump–probe detection based on time-resolved spectroscopy [4], nonlinear microscopy [5], optical parametric amplifiers [6]–[8], and coherent pulse synthesis [9]–[13], multiple ultra-short pulses with different wavelengths need to be injected into the same target, at the same time or with a specific time delay, to achieve the desired nonlinear effect. This means that pulses with different central wavelengths must be strictly synchronized. This is an extremely challenging problem, because of gain competition and the difficulties of achieving precise synchronization between optical pulses of different wavelengths.

Typically, in conventional multi-wavelength lasers, pulses at different wavelength oscillate in parallel within the same gain medium, and the multi-wavelength output is achieved by using different optical filters such as Mach–Zehnder filters [14]–[19], fiber comb filters [20], and fiber Bragg gratings (FBGs) [21], [22]. The problem with this type of laser is that because of the homogeneous broadening of the gain spectra of rare-earth-doped optical fibers, lasers at different wavelengths will compete for the gain [23]. In order to overcome this problem, low temperatures [24], [25] dual-core or elliptical fiber core [26], and frequency shifters [27], [28] have been strategically employed. But such device complexity and low-temperature working environments can be impractical. In addition, an ultra-short pulse usually has a wide spectrum, and hence when the central wavelengths of the desired multiple pulses are sufficiently close to each other, spectral interference is bound to occur. This is another major problem for conventional lasers.

Furthermore, for pulsed lasers, the synchronization of output pulses at different wavelengths is an even greater difficulty. In general, there are two types of synchronization schemes. The first is the active synchronization scheme [29]. Using a phase-locked loop [30] or optical cross correlation [31], one can synchronize two independent lasers. In [32], the synchronization of a femtosecond Ti:sapphire laser and a picosecond Nd: YVO_4 laser was achieved by using active synchronization, and accurate

The associate editor coordinating the review of this manuscript and approving it for publication was Zinan Wang.

synchronization with a time jitter lower than 1 ps was obtained. Another example of sub-picosecond active synchronization was achieved by the use of balanced optical cross-correlation (BOC) in passively mode-locked lasers [33]. However, active synchronization schemes of this type need accurate pulse detection and high-speed electronic feedback devices to control the repetition rate, making them complicated and expensive. In addition, synchronization accuracy needs to be improved [30]–[33]. The second type of synchronization scheme is passive synchronization, which can be based on various effects, such as cross-phase modulation (XPM) or cross-absorption modulation (XAM) [34]–[39]. Yoshitomi *et al.* used master–slave injection locking to achieve long-term stable synchronization between fiber lasers and Ti:sapphire mode-locked lasers [35], [36]. In [37], synchronous pulses were obtained from two ring-shaped cavities that shared a graphene saturable absorber. However, all of the abovementioned examples of synchronization involved multiple resonant cavities, and thus strict matching of cavity lengths is required. The typical mismatching tolerances are on the order of tens of microns [38], which makes the system sensitive to environmental perturbations, with typically poor stability [35]. In summary, a more practical solution for the synchronization of multi-wavelength pulsed lasers is needed.

In order to overcome the problems outlined above, a novel synchronous multi-wavelength fiber laser is proposed in this paper. Multi-stage cascaded Mamyshev regenerators [39] are used in the laser to form a single ring cavity (see Fig. 1). The offset filter of each regenerator in the cavity has a different central wavelength and thus switching between different wavelengths is realized in the cavity by the regenerators. This structure design inherently provides a guarantee of synchronization. Further, different laser wavelengths occupy different gain fibers, the gain competition and spectral interference caused by the overlap of filters in conventional multi-wavelength lasers are also avoided.

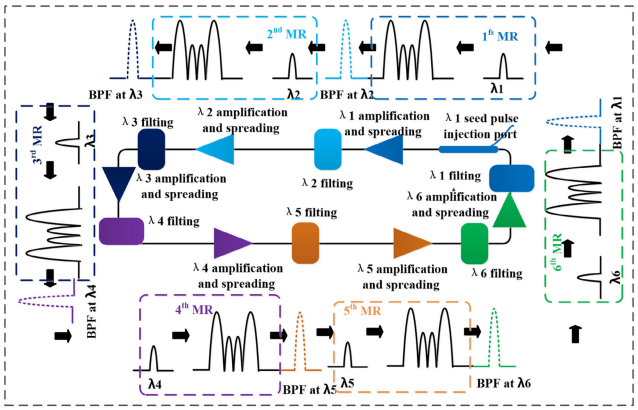

FIGURE 1. Schematic of a Mamyshev oscillator. The cavity comprises six Mamyshev regenerator (MR) arms, each containing a bandpass filter (BPF) centered at a different wavelength.

The feasibility of the system is verified by numerical simulation. The simulation results demonstrate that the system performs well and can operate stably under reasonable conditions with optimized parameters. After optimization, a six-wavelength synchronized laser with a repetition rate of 26.5 MHz (7.8 m cavity length), output peak power of 0.7 kW, and pulse duration of 0.4 ps is successfully realized. The six central wavelengths are 1035, 1040, 1045, 1050, 1055, and 1060 nm, and the spectral width in each case is 10 nm. The effects of the system parameters and the ordering of the wavelength filtering in the cavity are discussed. In order to confirm the capability of the system to provide multi-wavelength laser pulses with an arbitrary wavelength interval, a multi-wavelength laser with a 0.01 nm wavelength interval is also realized by numerical simulation.

II. NUMERICAL SIMULATION

A. WORKING PRINCIPLE OF THE MULTI-WAVELENGTH SYNCHRONOUS LASER

In previously reported studies, Mamyshev technology was used for mostly high-power pulse generation [40]–[42]. Exploiting the self-phase-modulation (SPM)-induced spectral broadening and offset spectral filtering of Mamyshev regeneration, unprecedented nonlinear phase shifts can be obtained, and higher peak powers can be achieved [43]. Here, we use this technology to generate multi-wavelength pulses, taking advantage of the inherent synchronization and gain-isolation conferred by the optical structures. Thus, the problems associated with the use of conventional technology for multi-wavelength synchronous ultra-short pulsed fiber lasers are solved.

The structure of a Mamyshev oscillator consisting of six cascaded Mamyshev regenerators [39], [44] is depicted schematically in Fig. 1. The cavity admits only high-intensity pulse. The pulse with sufficient nonlinear spectral broadening in each arm can bridge the spectral gap between two adjacent filters. A seed pulse with a center wavelength of λ_1 is injected into the laser cavity via a coupler, and it subsequently passes through the six-stage cascaded regenerator system. The functions of each regenerator stage are amplification (gain fiber), spectral broadening (gain fiber and following single-mode fiber), filtering (filter), and output (coupler). The gain fiber at every stage provides gain for only one of the multiple wavelengths. After seeding, the system is self-sustaining and stable, providing pulses with exactly the same repetition rate at six central wavelengths (λ_1, λ_2, λ_3, λ_4, λ_5, and λ_6). To further increase the number of output wavelengths, more regenerators can be cascaded.

For conventional multi-wavelength lasers, in which all wavelengths share a single gain fiber, gain competition is a problem. By contrast, the innovation of this laser consisting of multi-stage cascaded Mamyshev regenerators is that laser pulses of different wavelengths occupy different modules, rather than sharing the same gain medium. Thus, the mutual competition and crosstalk among the pulses of different wavelengths that occurs in conventional multi-wavelength lasers are effectively overcome.

Synchronization is considered a particularly difficult task for multi-wavelength pulsed lasers due to the difficulty of achieving exactly the same repetition rate. In the laser structure we propose, the laser pulse switches between different wavelengths as it travels around a single cavity, as shown in Fig. 1. Thus, the resulting pulses of different wavelengths correspond to the same cavity length, and have the same repetition rate, so the synchronization of the laser pulses is guaranteed inherently. As the delay between the output pulses at different wavelengths is determined by the fiber length between the output couplers in the cavity, there is inherent time delay between the pulses. In applications, we can adjust the delay of each wavelength with adjustable delay lines outside the laser cavity, according to demand, to guarantee the arrival of the pulses at a particular instrument or experiment at the same time or with a specific time difference.

B. CONSTRUCTION OF THE MULTI-WAVELENGTH SYNCHRONOUS LASER

The schematic of the six-wavelength laser system is shown in Fig. 2. The cavity comprises six Mamyshev regenerator arms, each containing a 0.3 m high concentration ytterbium-doped fiber (YDF) (nLight Yb1200 4/125, see the appendix for details), a bandpass filter (BPF), and an output coupler (OC). The coupling ratios of all the output couplers are 2:8 (out: in). A section of single-mode fiber (SMF) (Nufern 1060XP) and an optical isolator are placed between each of these regenerators. The isolators are used not only to guarantee unidirectional propagation, but also to prevent the formation of locally CW lasing caused by the reflection at junction points especially when non-fiber components (such as filters) with collimators are used. And the SMF is used to simulate the fiber of the optical fiber components between the regenerator modules. The influence of the SMF on the system will also be analyzed in Section II.D. The parameters of the optical fiber (SMF and YDF) used in the calculation are taken from the values provided by the commercial manufacturer. The numerical model and parameters of the simulation are summarized in the appendix. For optimized configuration, the center wavelengths of the filters corresponding to each stage are 1035, 1045, 1055, 1060, 1050, and 1040 nm, and the bandwidth is 10 nm for each case. The length of the SMF between each regenerator is 1 m. The simulated six-wavelength laser system operates in the all-normal dispersion regime with a cavity length of 7.8 m, corresponding to a repetition rate of 26.5 MHz.

For the optimized configuration, typically after approximately 50 round-trips through the cavity, the pulse reaches a steady state. Fig. 3(a) depicts the evolution of pulses in a stable state. The seed pulse with a center wavelength of 1035 nm is injected into the cavity (Fig. 2). The six-wavelength spectrum is shown in Fig. 3(b). We can see that the spectra of the pulses in the six-wavelength system overlap, but without disturbing with each other. The characteristics for the pulses of the six wavelengths are listed in Table 1.

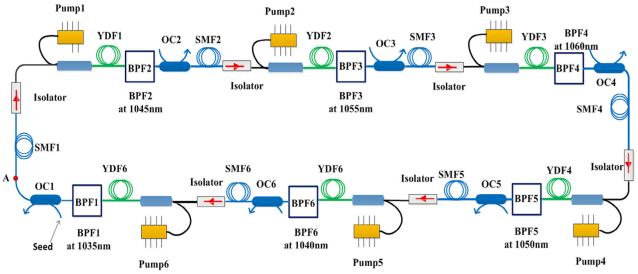

FIGURE 2. Schematic of the six-wavelength laser system (Point A is for open loop PTF calculation).

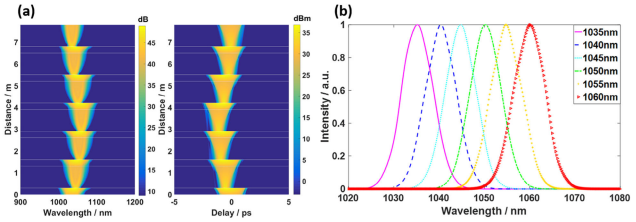

FIGURE 3. (a) Intracavity pulse evolution map, and (b) output spectra for the six pulses of the ring Mamyshev oscillator.

TABLE 1. Characteristics for the pulses of six wavelengths.

Wavelength (nm)	Bandwidth (nm)	Pulse duration (ps)	Intracavity Peak power (kW)	Output Peak power (kW)
1035	10	0.4347	2.841	0.710
1045	10	0.3907	3.143	0.786
1055	10	0.3810	3.072	0.768
1060	10	0.4005	3.075	0.769
1050	10	0.3663	3.251	0.813
1040	10	0.3965	2.963	0.741

Since the wavelengths of the filters of the Mamyshev regenerator are offset, there is no direct feedback path to self-start the laser. To induce pulsation in the laser cavity, a seed pulse is needed. The seed can be directed into the cavity by the coupler in Fig. 2. The startup thresholds for the seed pulses with different pulse durations and chirps are listed in Table 6 in the Appendix. The optimized laser described above has good stability characteristics. Once the laser starts and enters the stable working state, the pulse characteristics are only determined by the laser cavity parameters and do not depend on the pulse width and chirp of the seed pulse. In addition to Table 1, the laser pulse characteristics are also shown in Fig. 3 and Fig. 4.

C. DESIGN PRINCIPLES AND STABILITY CHARACTERISTICS

In addition to verifying the feasibility of the system, we have also studied its stability and summarized the design principles. We found that the open loop energy transfer

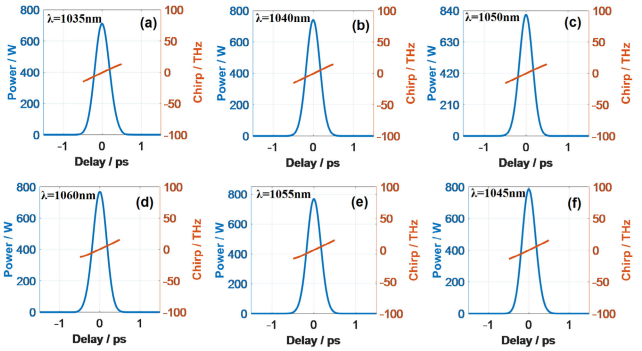

FIGURE 4. Time-domain characteristics for the six output wavelengths of the ring Mamyshev oscillator at the output port.

function (ETF) or the peak power transfer function (PTF) [3], [45] was the most important tool in the design of this system. Indeed, the shape of the PTF (which is more sensitive than ETF) is the key factor governing system performance.

Whether the system converges to a well-defined state is determined by the shape of the PTF, which must produce saturable absorption. As depicted in Fig. 5, the transfer function relating the output peak power, P_{out}, to the input peak power, P_{in}, must feature an inflection point. There are two intersection points (A and B) between the line of $P_{\text{in}} = P_{\text{out}}$ and the PTF. They are fixed points in nonlinear dynamics [46], where A is an unstable fixed point, and B is a stable fixed point. The low-power pulses (with peak power lower than the input peak power corresponding to point A), such as point C in Fig. 5, continuously lose power at the filtering stage. Meanwhile, the high-power pulses (with peak power higher than the input peak power corresponding to point A), such as point D and E in Fig. 5, stabilize toward a unique power value, the second point (point B), where the transfer function intersects with the straight line of $P_{\text{in}} = P_{\text{out}}$. Note that if the PTF is curved, oscillates, and intersects with $P_{\text{in}} = P_{\text{out}}$ line multiple time and there are more than one stable fixed points like the point B, the system is sensitive to initial conditions and is often characterized by instability and chaos [3], [46]. For our system, we obtained a stable intracavity pulse power at 2.8 kW, as shown in Fig. 6, corresponding to the second intersection of the PTF for 10 nm filter bandwidth in Fig. 7.

D. INFLUENCE OF THE FILTER BANDWIDTH AND THE SMF LENGTH IN THE CAVITY

We analyzed the influence of the Gaussian filter bandwidth on the six-wavelength laser system using the PTF. The resulting PTFs of the system with different filter bandwidths are plotted in Fig. 7. When the filter bandwidth is 10, 9, 8 and 7 nm, the system is stable with intracavity peak power of 2.8, 2.7, 2.5 and 2.3 kW, respectively, corresponding to the second point where the PTF curve intersects the straight line of $P_{\text{in}} = P_{\text{out}}$. As the bandwidth of the filters is reduced,

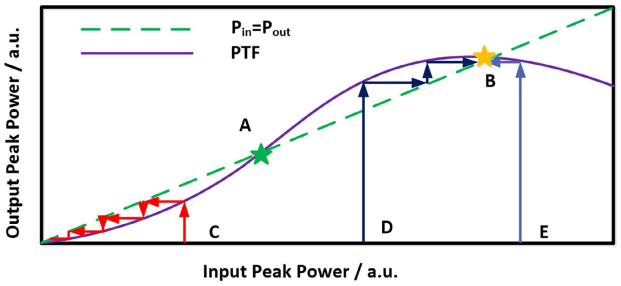

FIGURE 5. Peak power transfer function for the simulated ring Mamyshev system.

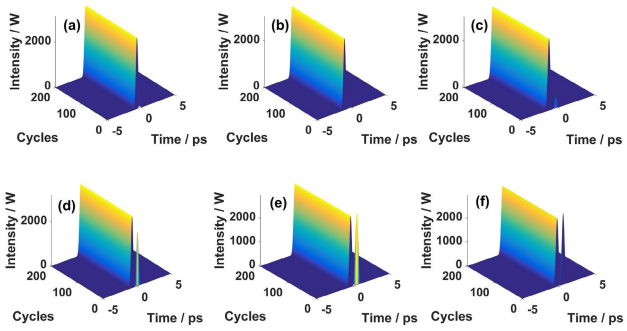

FIGURE 6. Time-domain intracavity pulse evolution maps for the six wavelengths. The central wavelengths of the six wavelengths are (a) 1035, (b) 1045, (c) 1055, (d) 1060, (e) 1050, and (f) 1040 nm.

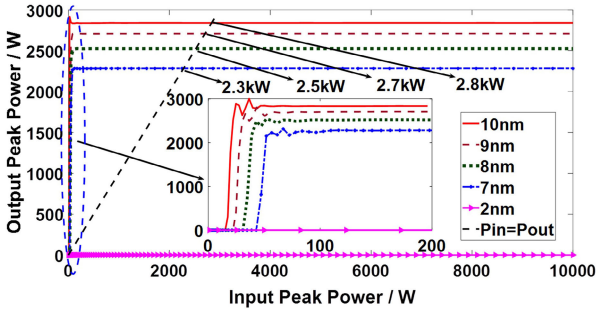

FIGURE 7. Six-wavelength system PTF diagram for different filter bandwidths.

the PTF curve of the system is shifted downward, as a whole. When the filter bandwidth is reduced to 2 nm, since the pulse energy is too small, and the amplification capability of the YDF is limited, the pulse cannot be amplified to a power level sufficient to maintain laser operation and the system stops working. It is notable that when the filter bandwidth is reduced to 7 nm, although from the PTF we can see that there is a laser in the system, the laser is not operating exactly at the six preset center wavelengths. The reduced bandwidth of the filter leads to a reduced energy for the filtered pulse, and the capacity of the filtered pulse to undergo spectral broadening decreases. The light pulse can no longer be broadened to the preset target wavelength position, but it can pass through the overlapping portion of the filter. When the gain

and loss reach a balance, the PTF curve will be formed, as shown in the figure, starting at the 7 nm bandwidth filter.

In addition to the above conclusions, in Section II.E we will show that the PTF is also affected by the flatness of the non-linearly broadened spectrum and the pass band of the filters. Pulses undergoing non-linear broadening will have a broad spectrum different spectral flatness at different wavelength positions, only when the filter is located within the smooth part of the spectrum, after nonlinear broadening, can the system run stably. It is necessary, therefore, to properly design the parameters of the system to meet this requirement.

All-fiber components, when they are used to construct lasers, are usually made of SMF; therefore, there must be a certain length of SMF between each regenerator in the laser cavity (Fig. 2). We analyzed the influence of the SMF fiber on the laser system using the PTF. The resulting PTFs of the system with different SMF fiber lengths are shown in Fig. 8.

The PTF curves in Fig. 8 indicate that a laser with a certain length of SMF can work well and stably; however, an excessively long SMF will cause a significant decrease in the peak power and make the PTF curve unstable. We calculated the evolution of the intracavity pulse, which was transmitted in the YDF, filtered by BPF (and attenuated by the coupler), and then entered the SMF (see Figs.9 - 12). Fig. 9 and Fig. 10 show the results for 1 m SMF, and Fig. 11 and Fig. 12 for 5 m SMF. In an SMF of an appropriate length,

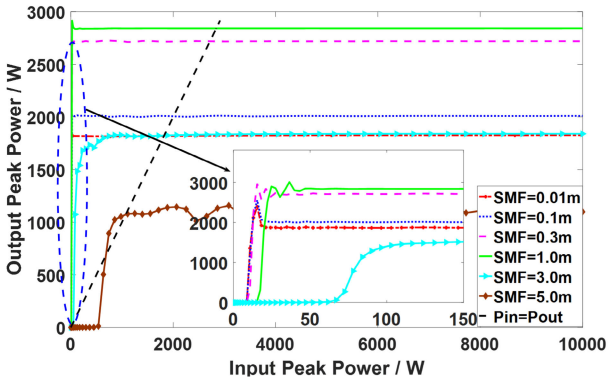

FIGURE 8. Six-wavelength system PTF diagram for different SMF lengths.

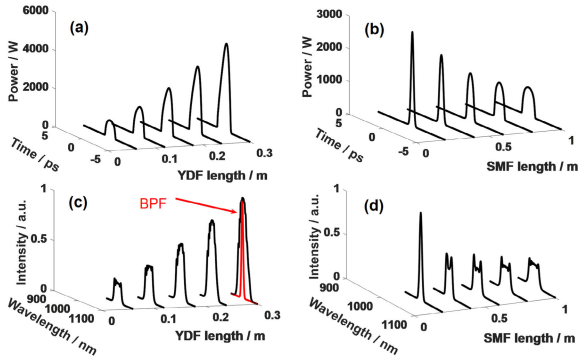

FIGURE 9. Pulse evolution in YDF and SMF for system with 1 m SMF.

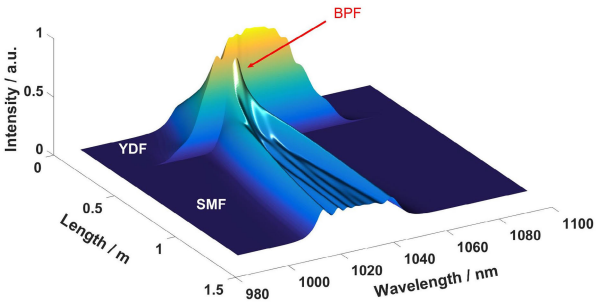

FIGURE 10. Pulse spectra evolution in YDF and SMF for system with 1 m SMF.

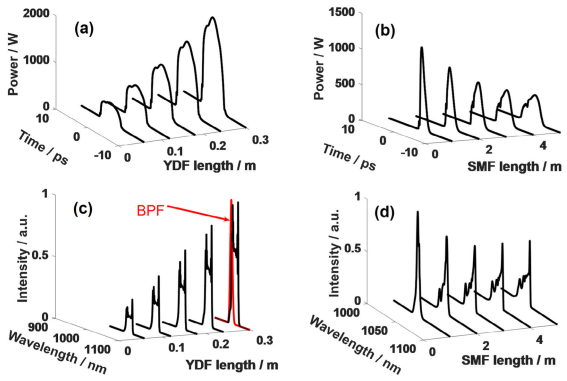

FIGURE 11. Pulse evolution in YDF and SMF for system with 5 m SMF.

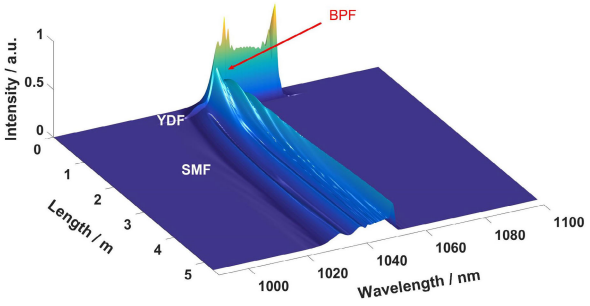

FIGURE 12. Pulse spectra evolution in YDF and SMF for system with 5 m SMF.

as shown in Fig. 9 and Fig. 10, the pulse spectrum is broadened, and it becomes flatter under the action of nonlinearity and normal dispersion. This is somewhat similar to the situation described in a previous study [47]. This makes the laser perform well. However, when the SMF between each regenerator is too long (5 m SMF), by comparing Figs. 9, 10 and Figs. 11, 12, we can see that the pulse spectrum before BPF filtering in the laser with 5 m SMF is much narrower than that with 1 m SMF. The spectral width before BPF filtering is reduced from ∼45 nm to ∼25 nm, and the output pulse duration becomes longer (increases from ∼0.4 ps to ∼2 ps); therefore, the spectral broadening is insufficient.

The filter pass band is at the edge of the pulse spectrum, and the pulse spectrum fails to fill the entire pass band of the filter (Fig. 11c and Fig. 12). This decreases the efficiency and deteriorates the spectrum. The dispersion-induced time domain pulse broadening and peak power reduction in the long SMF is the main reason for system degradation. When a long SMF must be used, one can consider increasing the gain of the amplifiers, because a higher pulse power is beneficial to the nonlinear broadening of the spectrum.

E. INFLUENCE OF WAVELENGTH ORDERING IN THE CAVITY

As mentioned previously, the laser pulse switches between different wavelengths as it travels in the cavity. Therefore, a design problem for a laser with the cascade structure is the wavelength arrangement. In order to investigate whether the arrangement of the different wavelengths within the cavity will influence the performance of the system, we simulated systems with different wavelength ordering. To compare the performance of the systems, two different wavelength orders were examined: (1) 1035, 1045, 1055, 1060, 1050, and 1040 nm (for λ_1 to λ_6, respectively, in Fig. 1 and Fig. 2, and (2) 1035, 1040, 1045, 1050, 1055, and 1060 nm (for λ_1 to λ_6, respectively, in Fig. 1). The system we analyzed earlier was in the first order. In this arrangement, most of the adjacent wavelength intervals are 10 nm (four of them are 10 nm, and two of them are 5 nm). Now we consider the system in the second order. First, most (five out of six) adjacent regenerators have a wavelength interval of 5 nm. However, because a feedback loop must be formed, a 25 nm wavelength span appears when switching from 1060 nm to 1035 nm. This is quite different from the system with the first sort order. Owing to the large difference in wavelength span, the configuration requirements of the YDF amplifier are different from the first order. That is, a smaller gain can be used for a small span, and a larger gain can be used for a large span. The gain of the amplifiers in simulation can be adjusted by setting the gain coefficient or YDF length. Here, we used a longer YDF of 0.4 m for large spans, and a 0.2 m YDF for small spans with the same gain coefficient.

The PTF curves for different SMF lengths for the second order wavelength arrangement are shown in Fig. 13. By comparing the PTF diagram of the two arrangement orders (Fig. 8 and Fig.13), it can be easily seen that the PTFs for most of the second arrangement order will have an oscillating curve. The curves oscillate strongly and have more than two intersections with the line $P_{\text{in}} = P_{\text{out}}$. As mentioned in our previous discussion, according to nonlinear dynamics, this result indicates that the stability of the second system is poor. We will discuss the stability of the laser and the reasons for this case in detail.

First, we analyze the impact of the oscillating PTF on the system. When the length of the SMF between each regenerator is short, the oscillating phenomenon of the PTF is more evident (Fig. 13); it allows us to see the impact of the oscillating PTF on laser characteristics more clearly.

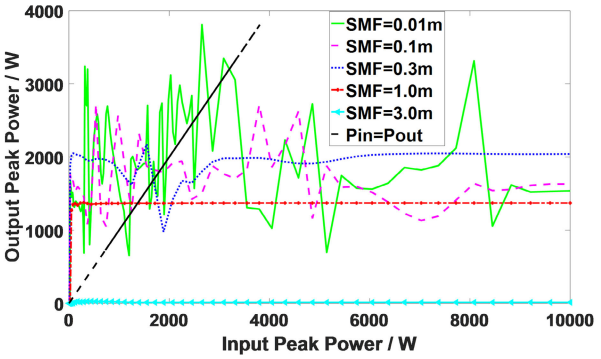

FIGURE 13. Six-wavelength system PTF diagram for different SMF length for the second order wavelength arrangement with 10 nm BPF bandwidth.

Therefore, we analyze this system with 0.01 m SMF as an example (Although such a short SMF is unrealistic for the system of all-fiber devices, the theoretical analysis will help us understand the problem more clearly because of its obvious characteristics). In order to test the stability of the system corresponding to the PTF that has multiple intersections with the line $P_{\text{in}} = P_{\text{out}}$, we investigated the output characteristics of the laser under different initial conditions (Fig. 14). A set of power values—308, 325.8, 326, 333.8, 400, and 491.9 W—was selected for the peak power of the starting seed pulse. We found that with initial seed pulse powers of 308, 400, and 491.9 W, the laser system was stable after several round-trips of the cavity, with 1.512 kW of output peak power. But with an initial seed pulse power of 325.8 W, the laser system is initially very unstable, and then reaches stability after about 155 round-trips of the cavity, with 1.512 kW of output peak power, as depicted in Fig. 15. However, with an initial seed pulse of 326 or 333.8 W, the laser system is always chaotic, as shown in Fig. 16. Analyzing this phenomenon, we found that for seed pulses having input powers of 325.8, 326, and 333.8 W, the output powers of the corresponding PTF curve are 3.14, 3.0, and 2.764 kW respectively, as depicted in Fig. 14(b), which means that the input power for the next cycle (next iteration) will fall into the oscillation zone at around ∼3 kW on the PTF curve. However, it can be seen

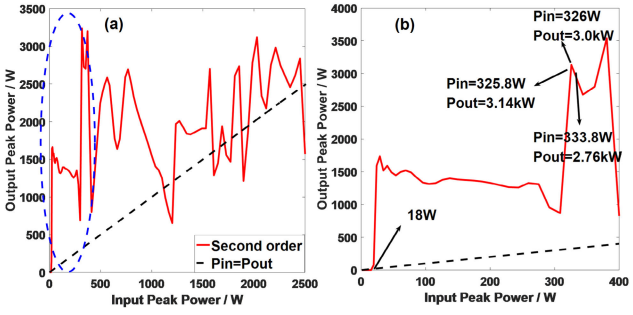

FIGURE 14. Expanded view of the transfer function in Fig. 13; the transfer function for the second order of wavelengths with 0.01 m SMF. (b) Expanded view of the area in (a) indicated by the dashed blue line.

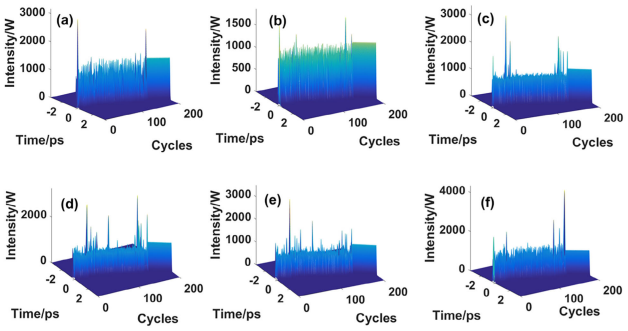

FIGURE 15. Time-domain intracavity pulse evolution maps for initial pulse peak power of 325.8 W. The central wavelengths of the six wavelengths are (a) 1035 nm, (b) 1040 nm, (c) 1045 nm, (d) 1050 nm, (e) 1055 nm, and (f) 1060 nm.

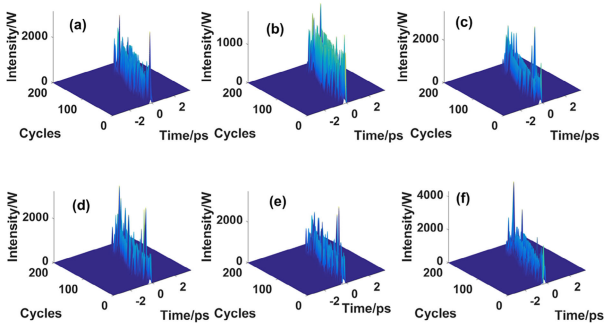

FIGURE 16. Time-domain intracavity pulse evolution maps for initial pulse peak power of 333.8 W. The central wavelengths of the six wavelengths are (a) 1035 nm, (b) 1040 nm, (c) 1045 nm, (d) 1050 nm, (e) 1055 nm, and (f) 1060 nm.

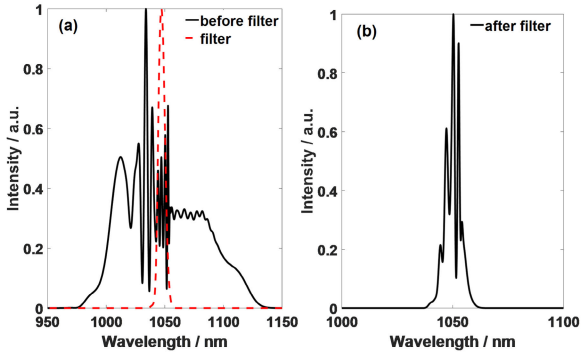

FIGURE 17. Spectrum before and after the BPF filter when the filter is located within an uneven part of the spectrum after nonlinear broadening.

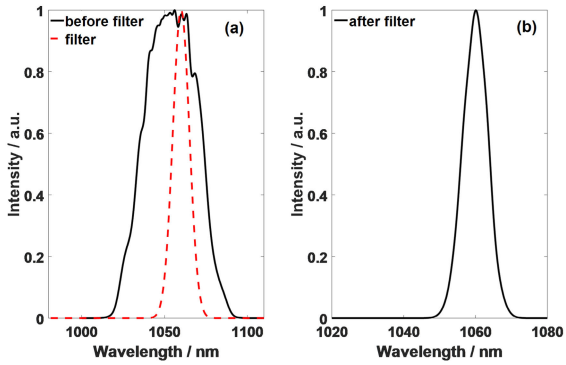

FIGURE 18. Spectrum before and after the BPF filter in the optimized configuration.

from the PTF in Fig. 13, and Fig. 14(a) that a state of severe oscillation of PTF is indicated for the input power region of ∼3 kW. By analyzing the laser system under this input power, it can be found that the pass band of the filter is located within an uneven part of the spectrum after nonlinear broadening (Fig. 17). (The spectrum before and after the filter of the optimized first order laser system which we have discussed before is shown in Fig. 18 for comparison). For this reason, the time-domain distortion of the pulse occurs, which eventually leads to system instability. Thus, when the PTF curve displays chaotic oscillations and multiple intersections with the line $P_{\text{in}} = P_{\text{out}}$, the corresponding laser system will be sensitive to the initial state according to the theory of nonlinear dynamics [46], and guaranteeing the final working state of the system will be difficult. Therefore, we should design the system to avoid such situations.

From the above-described results, it can be seen that choosing an appropriate power for the seed pulse results in the laser system being stabilized quickly at 1.512 kW. However, when the selected peak power of the seed pulse is far away from the stable point of the PTF curve of the system, the laser pulse power will fluctuate chaotically and endlessly between multiple states. Therefore, to ensure the system functions stably, the PTF curve should be smooth and have as few intersections (stable points) as possible (certainly, there is at least one) with the line $P_{\text{in}} = P_{\text{out}}$.

Next, we analyze the reasons for the degradation of the system with the second wavelength arrangement. In the six-wavelength system with wavelengths arranged in the second order, there is a large wavelength interval between the adjacent 1060 and 1035 nm modules. In order to understand the influence on the transfer function of each individual regenerator module, we calculated the transfer functions of the five-wavelength system (removing the 1035 nm module), the four-wavelength system (removing also the 1060 nm module), the three-wavelength system (removing also the 1055 nm module), and the two-wavelength system (removing, finally, also the 1050 nm module). The results of these simulations are shown in Fig. 19. It can be seen in Fig. 19(a) that after removing the largest wavelength-switch interval, the resultant PTF curve shows that the stability of the five-wavelength system is significantly improved, compared to the six-wavelength system in Fig. 19(b). Thus, we know that the drastic fluctuation of the curve for the second wavelength order is caused by the large wavelength gap, which results in the pass band of the filter being located at a part of the nonlinearly broadened spectrum that is not smooth, and hence it is not easy to stabilize the system.

Although the second order is likely to cause instability, stability can be achieved in a small range. We calculated the uniformity of the output pulses of the two systems with different wavelengths under the stable setting (1 m SMF).

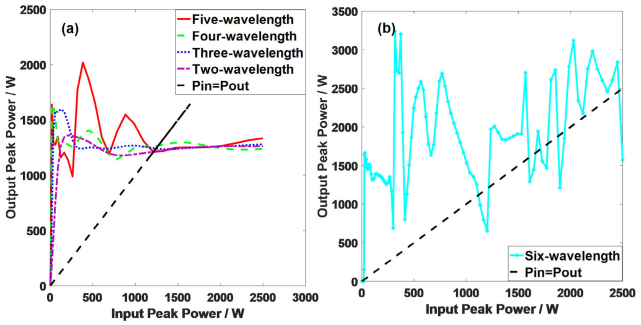

FIGURE 19. Transfer function graph of different wavelengths.

We found that the great difference in the wavelength span in the second order system will result in nonuniformity of the output pulse at different wavelengths. From Table 2, we can see that the pulse at 1035 nm is very different from the pulses at other wavelengths. The pulse at 1035 nm is just obtained after switching between the largest wavelength span (from 1060 nm to 1035 nm). This nonuniformity is very unfavorable for practical application.

TABLE 2. Characteristics for the pulses of six wavelengths of a second order system.

Wavelength (nm)	Bandwidth (nm)	Pulse duration (FWHM) (ps)	Intracavity peak power (kW)	Output peak power (kW)
1035	10	0.2833	1.359	0.3397
1040	10	0.4054	1.689	0.4223
1045	10	0.4200	2.048	0.5120
1050	10	0.4200	2.189	0.5473
1055	10	0.4200	2.167	0.5417
1060	10	0.4005	2.073	0.5182

In general, we can state that the smoothness of the PTF curve for the system arranged with the wavelength modules in the first order indicates that the laser is stable. Moreover, the requirements for the injected initial pulse in this case are not stringent; the power of the initial pulse can be selected from a large range because the system converges to one stable fixed point. By contrast, for the system arranged in the second order, the PTF curve fluctuates violently. This not only makes it difficult to achieve a stable functioning system, but also means that the system is very sensitive to the injected initial pulse power. In addition, more importantly, for the second order system, the significant difference in the wavelength span will result in considerable nonuniformity of the output pulse (pulse duration and peak power) for different wavelengths.

F. ARBITRARY WAVELENGTH INTERVAL OF THE MULTI-WAVELENGTH SYNCHRONOUS LASER

The ability to achieve an arbitrary wavelength interval is another advantage of this system. To demonstrate this, we designed a multi-wavelength pulsed laser with a very small wavelength interval using this new structure. In the numerical simulation, we selected 1035, 1045, 1055, 1060, 1054.99, and 1044.99 nm as the central wavelengths. The minimum interval of the central wavelength is 0.01 nm, the bandwidth of the filter is 10 nm and the SMF length is 1 m in each case. Fig. 20(a) depicts the evolution of pulses in the laser. The spectra of the six wavelengths are shown in Fig. 20(b). From the time-domain evolution (Fig. 21), it can be observed that the system runs stably for an extended period, and the characterization of the system is summarized in Table 3. The output results show that there is no interference between the outputs at the different wavelengths, which highlights the superiority of this laser and the newly designed structure.

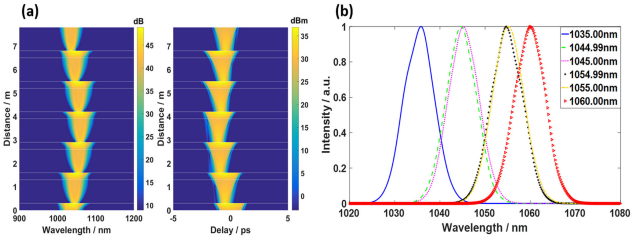

FIGURE 20. (a) Intracavity pulse evolution map and (b) output spectra for the six pulses of the ring Mamyshev oscillator with a minimum central-wavelength interval of 0.01 nm.

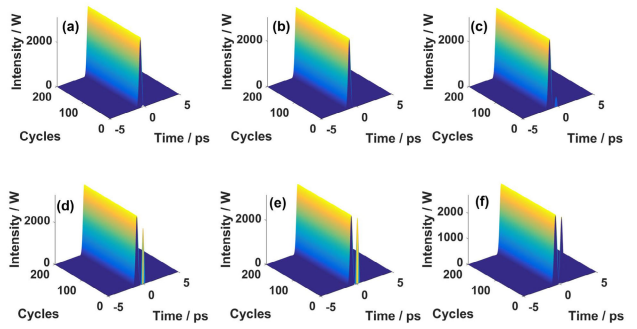

FIGURE 21. Time-domain pulse evolution maps for the ring Mamyshev oscillator with a minimum central-wavelength interval of 0.01 nm. The central wavelengths of the six wavelengths are (a) 1035, (b) 1045, (c) 1055, (d) 1060, (e) 1054.99, and (f) 1044.99 nm.

TABLE 3. Characteristics of the pulses of six wavelengths with a minimum central-wavelength interval of 0.01 nm.

Wavelength (nm)	Bandwidth (nm)	Pulse duration (FWHM) (ps)	Intracavity peak power (kW)	Output peak power (kW)
1035.00	10	0.4200	2.723	0.681
1045.00	10	0.3810	3.140	0.785
1055.00	10	0.3810	3.055	0.764
1060.00	10	0.4005	3.076	0.769
1054.99	10	0.3810	3.319	0.830
1044.99	10	0.3761	3.165	0.791

III. CONCLUSION

In conclusion, an ultra-short-pulse fiber laser based on a Mamyshev cavity was proposed. The laser can provide synchronous multi-wavelength pulses with overlapping spectra and an arbitrary center-wavelength interval. The designed structure was based on multi-stage cascaded nonlinear broadening and offset filtering, which helped to overcome the problems of gain competition, spectral interference, and difficulties in synchronization associated with conventional fiber lasers. Synchronous multi-wavelength pulsed lasers with 5 nm and even 0.01 nm output wavelength intervals were realized through numerical simulation. The pulses had spectral widths of 10 nm (greater than the interval between adjacent central wavelengths in the multi-pulse spectrum), and the system operated with ∼0.7 kW of output peak power and pulse durations of ∼0.4 ps. The PTF played a key role in the system design. This is an important tool for designing a stable laser and choosing seed pulses with appropriate powers for system start-up. We found that the bandpass range of the filter in the system must be located at the flat part of the nonlinearly broadened spectrum. In addition, the ordering of the modules for the different wavelengths within the cavity was also found to affect the PTF and the stability of the system. A reasonable arrangement of these wavelength modules, avoiding large wavelengths gaps between them, is conducive to ensuring that the built system is stable.

Note that the main objective of this article is to propose a new approach to generate synchronous multi-wavelength ultra-short pulses. Although this study focused on the all-fiber laser with all normal dispersion in the 1 μm band, this approach can be applied to other band and non-fiber devices such as integrated optical circuits. In addition, it is difficult to discuss all the details of the laser design in one article, there are still many interesting issues that need to be studied in future research.

APPENDIX

To simulate the propagation of the pulses in the fiber, the generalized nonlinear Schrödinger equation was solved. This includes the effects of attenuation, frequency dependent gain, dispersion, self-steepening, optical shock, and the Raman response [47], [48]:

$$\frac{\partial A}{\partial z}+\frac{a}{2}A-\frac{g}{2}A-\sum_{k\geq 2}\frac{i^{k+1}}{k!}\beta_k\frac{\partial^k A}{\partial T^k}=i\gamma\left(1+i\tau_{shock}\frac{\partial}{\partial T}\right)\times\left(A(z,T)\int_{-\infty}^{+\infty}R(T')\left|A(z,T-T')\right|^2dT'\right) \quad (1)$$

The profile of the gain spectrum was assumed to be Gaussian. The saturation of the gain fiber was also considered, and thus the gain coefficient in the frequency domain is:

$$g(\omega)=\frac{g_0}{1+E_{pulse}/E_{sat}}e^{-\left(\frac{\omega-\omega_0}{\omega_b}\right)^2} \quad (2)$$

where E_{pulse} is pulse energy, E_{sat} is the saturation energy, ω_0 is the reference frequency for 1050 nm, and ω_b is frequency for gain bandwidth (40 nm).

The simulation parameters were derived from the parameters of real optical fibers. For the gain fiber, we used a nLight liekki Yb1200 4/125 high concentration Ytterbium doped fiber with the absorption coefficient of 1200 dB/m at 976 nm. Usually a short length of this fiber (0.2-0.5 m) can be used to make an amplifier or laser in experiments [49]–[52]. The high gain coefficient and small core diameter of this fiber are beneficial for spectral broadening. For the SMF, a Nufern 1060XP single mode fiber is used. The dispersion parameters for YDF and SMF are listed in Table 4 and Table 5 (β_2 is taken from the values provided by the commercial manufacturer. β_3, β_4 and β_5 are derivative and high order derivative of β_2 with respect to angular frequency ω). In the simulation, the fifth-order dispersion coefficient was considered. The high-order dispersions are considered only for more accurate simulation. They are not the indispensable and necessary factors for laser operation and simulation. The nonlinear coefficient is 0.0104 $(\text{W}\cdot\text{m})^{-1}$ for the YDF, and 0.00497 $(\text{W}\cdot\text{m})^{-1}$ for the SMF. The gain coefficient g_0 for the YDF amplifier is 15 m^{-1}, the gain bandwidth is 40 nm, and the saturation energy is 3 nJ [39], [45], [53]. All the bandpass filters in the simulations are Gaussian filters with bandwidths of 10 nm.

TABLE 4. Dispersion parameter for YDF.

Wavelength (nm)	$\beta_2(\text{ps}^2/\text{m})$	$\beta_3(\text{ps}^3/\text{m})$	$\beta_4(\text{ps}^4/\text{m})$	$\beta_5(\text{ps}^5/\text{m})$
1035	2.27×10^{-2}	2.33×10^{-5}	-1.40×10^{-9}	-3.89×10^{-11}
1045	2.23×10^{-2}	2.35×10^{-5}	-7.06×10^{-10}	-4.13×10^{-11}
1055	2.19×10^{-2}	2.34×10^{-5}	2.05×10^{-11}	-4.37×10^{-11}
1060	2.17×10^{-2}	2.33×10^{-5}	3.94×10^{-10}	-4.50×10^{-11}
1050	2.21×10^{-2}	2.34×10^{-5}	-3.46×10^{-10}	-4.25×10^{-11}
1040	$2.25*10^{-2}$	2.34×10^{-5}	-1.06×10^{-9}	-4.01×10^{-11}

TABLE 5. Dispersion parameter for SMF.

Wavelength (nm)	$\beta_2(\text{ps}^2/\text{m})$	$\beta_3(\text{ps}^3/\text{m})$	$\beta_4(\text{ps}^4/\text{m})$	$\beta_5(\text{ps}^5/\text{m})$
1035	2.20×10^{-2}	3.47×10^{-5}	-2.83×10^{-8}	3.00×10^{-11}
1045	2.14×10^{-2}	3.52×10^{-5}	-2.88×10^{-8}	3.09×10^{-11}
1055	2.08×10^{-2}	3.57×10^{-5}	-2.94×10^{-8}	3.17×10^{-11}
1060	2.05×10^{-2}	3.59×10^{-5}	-2.96×10^{-8}	3.22×10^{-11}
1050	2.11×10^{-2}	3.54×10^{-5}	-2.91×10^{-8}	3.13×10^{-11}
1040	2.17×10^{-2}	3.49×10^{-5}	-2.86×10^{-8}	3.04×10^{-11}

(In Table 6, the "threshold power" is the power in the cavity after each output coupler (e.g. point A in Fig. 2). The seed power injected from the OC input port using the fiber coupler needs to be multiplied by 4.)

The seed is a linearly chirped Gaussian pulse, which can be written as [47]:

$$P(t)=P_0e^{-\left((1+iC)\frac{t^2}{T_0^2}\right)} \quad (3)$$

where P_0 is the peak power and T_0 is the pulse duration.

TABLE 6. Start up threshold for different kinds of seed pulses.

	T_0=0.25 ps	T_0=0.5 ps	T_0=1.0 ps	T_0=2.0ps
C = -2.0	2W	40W	260W	1.68×10^3W
C = -1.0	8W	43W	254W	1.64×10^3W
C = 0.0	15W	46W	250W	1.60×10^3W
C = 1.0	17W	48W	247W	1.57×10^3W
C = 2.0	10W	47W	245W	1.54×10^3W

From Table 6, we can see that shorter pulses are easier to spectrally broaden and thus easier to pass through Mamyshev's offset filter, therefore, they have smaller threshold powers. In addition, when pulse duration of the seed is small, the corresponding threshold is more susceptible to pulse chirp.

REFERENCES

[1] U. Keller, "Recent developments in compact ultrafast lasers," *Nature*, vol. 424, no. 6950, pp. 831–838, Sep. 2003.

[2] W. Fu, L. G. Wright, P. Sidorenko, S. Backus, and F. W. Wise, "Several new directions for ultrafast fiber lasers [invited]," *Opt. Express*, vol. 26, no. 8, pp. 9432–9463, Apr. 2018.

[3] H. Wei, B. Li, W. Shi, X. Zhu, R. A. Norwood, N. Peyghambarian, and S. Jian, "General description and understanding of the nonlinear dynamics of mode-locked fiber lasers," *Sci. Rep.*, vol. 7, no. 1, pp. 1292–1304, May 2017.

[4] Y. Terada, S. Yoshida, O. Takeuchi, and H. Shigekawa, "Real-space imaging of transient carrier dynamics by nanoscale pump–probe microscopy," *Nature Photon.*, vol. 4, no. 12, pp. 869–874, Oct. 2010.

[5] Y. Ozeki, W. Umemura, Y. Otsuka, S. Satoh, H. Hashimoto, K. Sumimura, N. Nishizawa, K. Fukui, and K. Itoh, "High-speed molecular spectral imaging of tissue with stimulated Raman scattering," *Nature Photon.*, vol. 6, no. 12, pp. 845–851, Nov. 2012.

[6] C. Y. Teisset, N. Ishii, T. Fuji, T. Metzger, and F. Krausz, "Soliton-based pump-seed synchronization for few-cycle OPCPA," *Opt. Express*, vol. 13, no. 17, pp. 6550–6557, Sep. 2005.

[7] D. Yoshitomi, X. Zhou, Y. Kobayashi, S. Satoh, H. Hashimoto, K. Sumimura, N. Nishizawa, K. Fukui, and K. Itoh, "Long-term stable passive synchronization of 50 μJ femtosecond Yb-doped fiber chirped-pulse amplifier with a mode-locked Ti: Sapphire laser," *Opt. Express*, vol. 18, no. 25, pp. 26027–26036, Dec. 2010.

[8] A. Schwarz, M. Ueffing, Y. Y. Deng, X. Gu, H. Fattahi, T. Metzger, M. Ossiander, F. Krausz, and R. Kienberger, "Active stabilization for optically synchronized optical parametric chirped pulse amplification," *Opt. Express*, vol. 20, no. 5, pp. 5557–5565, Feb. 2012.

[9] R. K. Shelton, L. S. Ma, H. C. Kapteyn, M. M. Murnane, J. L. Hall, and J. Ye, "Phase-coherent optical pulse synthesis from separate femtosecond lasers," *Science*, vol. 293, no. 5533, pp. 1286–1289, Sep. 2001.

[10] D. Yoshitomi, Y. Kobayashi, and K. Torizuka, "Characterization of Fourier-synthesized optical waveforms from optically phase-locked femtosecond multicolor pulses," *Opt. Lett.*, vol. 33, no. 24, pp. 2925–2927, Jan. 2008.

[11] J. A. Cox, W. P. Putnam, A. Sell, A. Leitenstorfer, and F. X. Kärtner, "Pulse synthesis in the single-cycle regime from independent mode-locked lasers using attosecond-precision feedback," *Opt. Lett.*, vol. 37, no. 17, pp. 3579–3581, Sep. 2012.

[12] G. Krauss, S. Lohss, T. Hanke, A. Sell, S. Eggert, R. Huber, and A. Leitenstorfer, "Synthesis of a single cycle of light with compact erbium-doped fibre technology," *Nature Photon.*, vol. 4, no. 1, pp. 33–36, Jan. 2010.

[13] D. J. Jones, K. W. Holman, M. Notcutt, J. Ye, J. Chandalia, L. A. Jiang, E. P. Ippen, and H. Yokoyama, "Ultralow-jitter, 1550-nm mode-locked semiconductor laser synchronized to a visible optical frequency standard," *Opt. Lett.*, vol. 28, no. 10, pp. 813–815, Jun. 2003.

[14] H. Takahashi, H. Toba, and Y. Inoue, "Multiwavelength ring laser composed of EDFAs and an arrayed-waveguide wavelength multiplexer," *Electron. Lett.*, vol. 30, no. 1, pp. 44–45, Jan. 1994.

[15] T. Miyazaki, N. Edagawa, S. Yamamoto, and S. Akiba, "A multiwavelength fiber ring-laser employing a pair of silica-based arrayed-waveguide-gratings," *IEEE Photon. Technol. Lett.*, vol. 9, no. 7, pp. 910–912, Jul. 1997.

[16] N. Park, J. W. Dawson, and K. J. Vahala, "Multiple wavelength operation of an erbium-doped fiber laser," *IEEE Photon. Technol. Lett.*, vol. 4, no. 6, pp. 540–541, Jun. 1992.

[17] H. L. An, X. Z. Lin, H. D. Liu, E. Y. B. Pun, and P. S. Chung, "Multiwavelength erbium-doped fiber laser incorporating a double-pass Mach–Zehnder interferometer," *Microw. Opt. Technol. Lett.*, vol. 20, no. 4, pp. 270–272, Feb. 1999.

[18] H. L. An, X. Z. Lin, E. Y. B. Pun, and H. D. Liu, "Multi-wavelength operation of an erbium-doped fiber ring laser using a dual-pass Mach–Zehnder comb filter," *Opt. Commun.*, vol. 169, nos. 1–6, pp. 159–165, Oct. 1999.

[19] J. J. Veselka and S. K. Korotky, "A multiwavelength source having precise channel spacing for WDM systems," *IEEE Photon. Technol. Lett.*, vol. 10, no. 7, pp. 958–960, Jul. 1998.

[20] J. Chow, G. Town, B. Eggleton, M. Ibsen, K. Sugden, and I. Bennion, "Multiwavelength generation in an erbium-doped fiber laser using in-fiber comb filters," *IEEE Photon. Technol. Lett.*, vol. 8, no. 1, pp. 60–62, Jan. 1996.

[21] A. D. Kersey and W. W. Morey, "Multi-element Bragg-grating based fibre-laser strain sensor," *Electron. Lett.*, vol. 29, no. 11, pp. 964–966, Jun. 1993.

[22] E. Achaerandio, S. Jarabo, S. Abad, and M. Lopez-Amo, "New WDM amplified network for optical sensor multiplexing," *IEEE Photon. Technol. Lett.*, vol. 11, no. 12, pp. 1644–1646, Dec. 1999.

[23] Q. Mao and J. W. Y. Lit, "Multiwavelength erbium-doped fiber lasers with active overlapping linear cavities," *J. Lightw. Technol.*, vol. 21, no. 1, pp. 160–169, Jan. 2003.

[24] S. Yamashita and K. Hotate, "Multiwavelength erbium-doped fiber laser using intracavity etalon and cooled by liquid nitrogen," *Electron. Lett.*, vol. 32, no. 14, pp. 1298–1299, Aug. 1996.

[25] S. Yamashita, K. Hsu, and W. H. Loh, "Miniature erbium:Ytterbium fiber Fabry–Pérot multiwavelength lasers," *IEEE J. Sel. Topics Quantum Electron.*, vol. 3, no. 4, pp. 1058–1064, Sep. 1997.

[26] O. Graydon, W. H. Loh, R. I. Laming, and L. Dong, "Triple-frequency operation of an er-doped twincore fiber loop laser," *IEEE Photon. Technol. Lett.*, vol. 8, no. 1, pp. 63–65, Feb. 1996.

[27] A. Bellemare, M. Karasek, M. Rochette, S. LaRochelle, and M. Tetu, "Room temperature multifrequency erbium-doped fiber lasers anchored on the ITU frequency grid," *J. Lightw. Technol.*, vol. 18, no. 6, pp. 825–831, Jun. 2000.

[28] S. K. Kim, M. J. Chu, and J. H. Lee, "Wideband multiwavelength erbium-doped fiber ring laser with frequency shifted feedback," *Opt. Commun.*, vol. 190, nos. 1–6, pp. 291–302, Apr. 2001.

[29] H. Tian, Y. Song, J. Yu, S. Shi, and H. Hu, "Optical-optical synchronization between two independent femtosecond Yb-fiber lasers with 10–20 instability in 105 S," *IEEE Photon. J.*, vol. 9, no. 5, pp. 3200607–3200615, Sep. 2017.

[30] R. K. Shelton, S. M. Foreman, L. S. Ma, J. L. Hall, H. C. Kapteyn, M. M. Murnane, M. Notcutt, and J. Ye, "Subfemtosecond timing jitter between two independent, actively synchronized, mode-locked lasers," *Opt. Lett.*, vol. 27, no. 5, pp. 312–314, Mar. 2002.

[31] T. Miura, H. Nagaoka, K. Takasago, K. Kobayashi, A. Endo, K. Torizuka, M. Washio, and F. Kannari, "Active synchronization of two mode-locked lasers with optical cross correlation," *Appl. Phys. B, Lasers Opt.*, vol. 75, no. 1, pp. 19–23, Jul. 2002.

[32] P. Wang, H. Zhao, Z. H. Wang, D. H. Li, and Z. Y. Zhi, "Active synchronization of two independent femtosecond and picosecond lasers and sum frequency generation of two laser pulses," *Acta Phys. Sin.*, vol. 55, no. 8, pp. 4161–4165, Aug. 2006.

[33] T. R. Schibli, J. Kim, O. Kuzucu, J. T. Gopinath, S. N. Tandon, G. S. Petrich, L. A. Kolodziejski, J. G. Fujimoto, E. P. Ippen, and F. X. Kaertner, "Attosecond active synchronization of passively mode-locked lasers by balanced cross correlation," *Opt. Lett.*, vol. 28, no. 11, pp. 947–949, Jul. 2003.

[34] C. Y. Guo, W. Q. Liu, S. C. Ruan, J. Yu, Y. W. Chen, P. G. Yan, J. Z. Wang, S. Jain, and P. Hua, "Tunable passively-synchronized 1-μm Q-switched and 1.5-μm gain-switched dual-wavelength fiber laser based on an Er/Yb codoped fiber," *IEEE Photon. J.*, vol. 9, no. 3, pp. 1502609–1502618, Jun. 2017.

[35] D. Yoshitomi and K. Torizuka, "Long-term stable passive synchronization between two-color mode-locked lasers with the aid of temperature stabilization," *Opt. Express*, vol. 22, no. 4, pp. 4091–4097, Feb. 2014.

[36] K. Huang, J. Zeng, J. W. Gan, Q. Hao, M. Yan, and H. Zeng, "Passive all-optical synchronization for polarization-maintaining mode-locked fiber lasers," *Opt. Express*, vol. 26, no. 24, pp. 32184–32193, Nov. 2018.
[37] J. Sotor, G. Sobon, J. Tarka, I. Pasternak, A. Krajewska, W. Strupinski, and K. M. Abramski, "Passive synchronization of erbium and thulium doped fiber mode-locked lasers enhanced by common graphene saturable absorber," *Opt. Express*, vol. 22, no. 5, pp. 5536–5543, Mar. 2014.
[38] D. Yoshitomi, Y. Kobayashi, M. Kakehata, H. Takada, K. Torizuka, T. Onuma, H. Yokoi, T. Sekiguchi, and S. Nakamura, "Ultralow-jitter passive timing stabilization of a mode-locked Er-doped fiber laser by injection of an optical pulse train," *Opt. Lett*, vol. 31, no. 22, pp. 3243–3245, Dec. 2006.
[39] P. V. Mamyshev, "All-optical data regeneration based on self-phase modulation effect," in *Proc. IEEE Conf. Opt. Commun.*, Sep. 1998, pp. 475–476.
[40] K. Regelskis, J. Želudevičius, K. Viskontas, and G. Račiukaitis, "Ytterbium-doped fiber ultrashort pulse generator based on self-phase modulation and alternating spectral filtering," *Opt. Lett.*, vol. 40, no. 22, pp. 5255–5258, Nov. 2015.
[41] P. Sidorenko, W. Fu, L. G. Wright, M. Olivier, and F. W. Wise, "Self-seeded, multi-megawatt, Mamyshev oscillator," *Opt. Lett.*, vol. 43, no. 11, pp. 2672–2675, May 2018.
[42] W. Liu, R. Liao, J. Zhao, J. Cui, Y. Song, C. Wang, and M. Hu, "Femtosecond Mamyshev oscillator with 10-MW-level peak power," *Optica*, vol. 6, no. 2, pp. 194–197, Feb. 2019.
[43] Z. Liu, Z. M. Ziegler, L. G. L. G. Wright, and F. W. Wise, "Megawatt peak power from a Mamyshev oscillator," *Optica*, vol. 4, no. 6, pp. 649–654, Jun. 2017.
[44] S. Pitois, C. Finot, and L. Provost, "Asymptotic properties of incoherent waves propagating in an all-optical regenerators line," *Opt. Lett.*, vol. 32, no. 22, pp. 3263–3265, Dec. 2007.
[45] T. North and C.-S. Brès, "Regenerative similariton laser," *APL Photon.*, vol. 1, no. 2, pp. 021302–021309, May 2016.
[46] S. H. Strogatz, "One dimentional maps," in *Nonlinear Dynamics and Chaos: With Applications to Physics, Biology Chemistry and Engineering*, 2nd ed. Boca Raton, FL USA: CRC Press, 2018 pp. 355–404.
[47] G. P. Agrawal, "'Pulse propagation in fibers' and 'effect of group-velocity dispersion,'" in *Nonlinear Fiber Optics*, 5th ed. San Francisco, CA, USA: Academic, 2013, pp. 27–56 and 103–104.
[48] J. M. Dudley and J. R. Taylor, "Nonlinear fibre optics overview," in *Supercontinuum Generation in Optical Fiber*, 1st ed. Cambridge, U.K.: Cambridge Univ. Press, 2010, pp. 32–51.
[49] Y. Huang, F. Shi, T. Wang, X. Liu, X. Zeng, F. Pang, T. Wang, and P. Zhou, "High-order mode Yb-doped fiber lasers based on mode-selective couplers," *Opt. Express*, vol. 55, no. 15, pp. 19171–19181. Jul. 2018.
[50] S. W. Moore, D. B. S. Soh, S. E. Bisson, B. D. Patterson, and W. L. Hsu, "400 μJ 79 ns amplified pulses from a Q-switched fiber laser using an Yb^{3+}-doped fiber saturable absorber," *Opt. Express*, vol. 20, no. 21, pp. 23778–23789, Oct. 2012.
[51] Z. H. Yu, W. Shi, X. Dong, J. Li, Y. Zhao, and H. Liu, "110 W all-fiber picosecond master oscillator power amplifier based on large-core-diameter ytterbium-doped fiber," *Appl. Opt.*, vol. 55, no. 15, pp. 4119–4122, May 2016.
[52] P. Li, A. Wang, and X. Wang, "330 MHz, sub 50 fs Yb: Fiber ring laser," *Opt. Commun.*, vol. 285, no. 9, pp. 2430–2432, May 2012.
[53] R. Paschotta, J. Nilsson, A. C. Tropper, and D. C. Hanna, "Ytterbium-doped fiber amplifiers," *IEEE J. Quantum Electron.*, vol. 33, no. 7, pp. 1049–1056, Jul. 1997.

RONGHUA LI received the B.S. degree in electronic information engineering from Qingdao University, in 2017. She is currently pursuing the M.S. degree with the Institute of Lightwave Technology, Beijing Jiaotong University. Her research interests include fiber optics and nonlinear fiber optics.

HUAI WEI received the Ph.D. degree from Beijing Jiaotong University, Beijing, China, in 2004.

He joined the Key Laboratory of All Optical Network and Advanced Telecommunication Network of EMC, Institute of Lightwave Technology, Beijing Jiaotong University, in 2004, where he has been an Associate Professor since 2006. He was a Visiting Researcher with the College of Optical Sciences, The University of Arizona, Tucson, AZ, USA, in 2010. He was also a Visiting Researcher with the FEMTO-ST Institute, Besançon, France, from 2019 to 2020. His research interests include ultrafast optics, fiber lasers, and nonlinear fiber optics.

WEIXUAN QIN received the M.S. degree from the Institute of Lightwave Technology, Beijing Jiaotong University, in 2019. His research interests include ultrafast optics and nonlinear fiber optics.

ZEHANG MA received the B.S. degree in electronic information engineering from Beijing Jiaotong University, in 2019, where he is currently pursuing the M.S. degree with the Institute of Lightwave Technology. His research interests include fiber optics and nonlinear fiber optics.

CHENGTIAN TANG received the B.S. degree in electronic information engineering from Qingdao University, in 2018. He is currently pursuing the M.S. degree with the Institute of Lightwave Technology, Beijing Jiaotong University. His research interests include fiber optics and nonlinear fiber optics.

BIN LI received the bachelor's degree in communication engineering from Northern Jiaotong University, Beijing, in 2001, and the Ph.D. degree in optical fiber communication from the Institute of Lightwave Technology, Beijing Jiaotong University, in 2007. Since 2008, she has been an Associate Professor with the School of Information and Communication Engineering, Communication University of China. From September 2014 to October 2015, she was a Visiting Researcher with the College of Optical Sciences, The University of Arizona, USA. Her current research interests include optical fiber communication, fiber lasers, and terahertz components.

LI PEI received the M.S. degree in optical fiber communication and the Ph.D. degree in telecommunications and information systems from Beijing Jiaotong University, in 1998 and 2002, respectively. Since 2004, she has been a Professor with the Key Laboratory of All Optical Network and Advanced Telecommunication Network, Beijing Jiaotong University. Her research interests include high-speed optical telecommunication networks, optical fiber sensor, key technology of optical fiber communication, ROF, and so on.